

FOURTH ORDER ACCURATE COMPACT SCHEME FOR FIRST-ORDER MAXWELL'S EQUATIONS

I. VERSANO, E. TURKEL, AND S. TSYNKOV

ABSTRACT. We construct a compact fourth-order scheme, in space and time, for the time-dependent Maxwell's equations given as a first-order system on a staggered (Yee) grid. At each time step, we update the fields by solving positive definite second-order elliptic equations. We face the challenge of finding compatible boundary conditions for these elliptic equations while maintaining a compact stencil. The proposed scheme is compared computationally with a non-compact scheme and data-driven approach.

Keywords: Compact finite differences, Maxwell's equations, High order accuracy.

Acknowledgments

The work supported by the US–Israel Bi-national Science Foundation (BSF) under grant # 2020128.

1. INTRODUCTION

Time-dependent Maxwell's equations have been established for over 125 years as the theoretical representation of electromagnetic phenomena [10, 11]. However, the accuracy requirement of high-frequency simulations remains a challenge due to a pollution effect which has been discovered firstly for the convection equation [8] and later on for the Helmholtz equation [1, 5]. The pollution effect states that, for a p order time accurate scheme, the quantity $\omega^{p+1}h_T^p$ should remain constant in order for the error to remain constant as the wave-number ω varies. A similar phenomenon applies also to spatial errors [1, 5]. This effect motivates the need for higher order schemes, i.e., larger p . Using straightforward central differences, higher-order accuracy requires a larger stencil. This has two disadvantages. Firstly, the larger the stencil, the more work may be needed to invert a matrix with a larger bandwidth and more non-zero entries. Even more serious are the difficulties near boundaries. A large stencil requires some modification near the boundaries where all the points needed in the stencil are not available. This raises questions about the efficiency and stability of such schemes. In addition, higher-order compact methods can achieve the same error while using fewer grid nodes, making them more efficient in terms of both storage and CPU time than non-compact or low-order methods (see e.g., [3] for the wave equation, [14] for Helmholtz equation, [18, 19] for Maxwell's equations, and references therein). The Yee scheme (also known as finite-difference time-domain, or FDTD) was introduced by Yee [17] and remains the common numerical method used

for electromagnetic simulations [16]. Although it is only a second-order method, it is still preferred for many applications because it preserves important structural features of Maxwell's equations that other methods fail to capture. One of the main novelties presented by Yee was the staggered-grid approach, where the electric field \mathbf{E} and magnetic field \mathbf{H} do not live at the same discrete space or time locations but at separate nodes on a staggered lattice. From the perspective of differential forms in space-time, it becomes clear that the staggered-grid approach is more faithful to the structure of Maxwell's equations that are dual to one another and hence \mathbf{E}, \mathbf{H} naturally live on two staggered, dual meshes [15]. The question of staggered versus non-staggered high-order schemes has been studied in [7] (see also [16, pages 63-109]), where it has been shown that, for a given order of accuracy, a staggered scheme is more accurate and efficient than a non-staggered scheme.

In this paper, we present a new compact fourth-order accurate scheme, in both space and time, for Maxwell's equations in three dimensions using an equation-based method on a staggered grid. At each time step, we update the solution by solving uncoupled (positive definite) second-order elliptic equations using the conjugate gradient method. This procedure involves a non-trivial treatment at the boundaries on which boundary conditions are not given explicitly and have to be deduced by the equation itself while maintaining the compact stencil. While the development of the scheme is done in 3D, the simulations are only two-dimensional for the sake of simplicity.

1.1. Maxwell's equations. Let $\mathbf{E}, \mathbf{H}, \mathbf{D}, \mathbf{B}, \mathbf{J}$ be (real-valued) vector fields, defined for $(t, \mathbf{x}) \in [0, \infty) \times \Omega$, which take values in \mathbb{R}^3 . The Maxwell equations, in first-order differential vector form, are given by

$$\begin{aligned} \frac{\partial \mathbf{D}}{\partial t} &= \nabla \times \mathbf{H} - \mathbf{J}, & \frac{\partial \mathbf{B}}{\partial t} &= -\nabla \times \mathbf{E} \\ \nabla \cdot \mathbf{H} &= 0 & \nabla \cdot \mathbf{E} &= \frac{\rho}{\epsilon} \\ \mathbf{B} &= \mu \mathbf{H} & \mathbf{D} &= \epsilon \mathbf{E} \end{aligned} \tag{1.1}$$

in Ω , where in addition

$$\frac{\partial \rho}{\partial t} + \nabla \cdot \mathbf{J} = 0.$$

Here $\nabla \times$ denotes the curl operator with respect to \mathbf{x} . We assume that smooth initial conditions are given for \mathbf{D} and \mathbf{B} at $t = 0$. We assume the following:

- (1) μ, ϵ are positive constants, unless noted otherwise, satisfying $\frac{1}{\mu\epsilon} = c^2$.
- (2) $\Omega = [0, 1]^3$, $\vec{n} \times \mathbf{E} = 0$ on $\partial\Omega$ ([12, Section 8]).

The identity $\nabla \cdot (\nabla \times) = 0$ implies that $\frac{\partial}{\partial t} (\nabla \cdot \mathbf{H}) = 0$ and hence the divergence conditions are only restrictions on the initial conditions. By letting $\tau = ct$, $Z = \sqrt{\mu/\epsilon}$, we obtain the

following re-scaled equations:

$$\frac{\partial \mathbf{E}}{\partial \tau} = Z(\nabla \times \mathbf{H} - \mathbf{J}) \quad \text{in } (0, \infty) \times \Omega \quad (1.2a)$$

$$\frac{\partial \mathbf{H}}{\partial \tau} = -\frac{1}{Z} \nabla \times \mathbf{E} \quad \text{in } (0, \infty) \times \Omega \quad (1.2b)$$

$$\nabla \cdot \mathbf{H}(\tau, x, y, z) = 0 \quad (1.2c)$$

$$\nabla \cdot \mathbf{E}(\tau, x, y, z) = \frac{\rho}{\varepsilon} \quad (1.2d)$$

$$\frac{1}{c} \frac{\partial \rho}{\partial \tau} + \nabla \cdot \mathbf{J} = 0. \quad (1.2e)$$

This is supplemented by the initial conditions

$$\mathbf{E}(0, x, y, z) = \mathbf{E}_0, \quad \mathbf{H}(0, x, y, z) = \mathbf{H}_0$$

and the boundary conditions $\vec{n} \times \mathbf{E} = 0$ on $\partial\Omega$.

Remark 1.1. *Differentiating (1.2) with respect to τ , we see that \mathbf{E} and \mathbf{H} satisfy the wave equation*

$$\begin{aligned} \frac{\partial^2 \mathbf{E}}{\partial \tau^2} &= -Z \frac{\partial \mathbf{J}}{\partial \tau} - \nabla \times \nabla \times \mathbf{E} \\ &= -Z \frac{\partial \mathbf{J}}{\partial \tau} - \nabla(\nabla \cdot \mathbf{E}) + \Delta \mathbf{E} \\ &= -Z \frac{\partial \mathbf{J}}{\partial \tau} - \nabla(\nabla \cdot \mathbf{E}) + \Delta \mathbf{E} \end{aligned} \quad (1.3)$$

and

$$\frac{\partial^2 \mathbf{H}}{\partial \tau^2} = -\nabla \times \nabla \times \mathbf{H} - \nabla \times \partial_\tau \mathbf{J} = \Delta \mathbf{H} - \nabla \times \partial_\tau \mathbf{J}. \quad (1.4)$$

Here Δ denotes the Laplacian with respect to \mathbf{x} .

To determine the number of imposed boundary conditions, we need to examine the eigenvalues for the reduced one-dimensional equations at that boundary. A positive eigenvalue indicates a variable that is entering from outside the domain and so needs to be specified. A negative eigenvalue indicates the variable is determined from the inside and so cannot be imposed and instead is determined by the interior equations. A zero eigenvalue is more ambiguous.

Remark 1.2. *An imposed boundary condition must contain only derivatives of a lower order than the differential equation. Thus, for a first-order system, all boundary conditions must be of Dirichlet type. A Neumann condition is **not** considered an imposed boundary condition.*

To derive the boundary conditions for \mathbf{E} and \mathbf{H} , we analyze the characteristics of the homogeneous counterpart to system (1.1), $\rho = 0$ and $\mathbf{J} = 0$, in the direction normal to

the boundary (cf. [6, Section 9.1]). The two divergence equations can be considered as constraints on the initial data and do not affect the characteristics. Let w be the vector $(E_x, E_y, E_z, H_x, H_y, H_z)^t$. Then, considering only the x space derivatives (without loss of generality) we arrive at

$$\frac{\partial w}{\partial t} = Aw_x$$

where

$$A = \begin{pmatrix} 0 & 0 & 0 & 0 & 0 & 0 \\ 0 & 0 & 0 & 0 & 0 & \frac{1}{\epsilon} \\ 0 & 0 & 0 & 0 & -\frac{1}{\epsilon} & 0 \\ 0 & 0 & 0 & 0 & 0 & 0 \\ \frac{1}{\mu} & 0 & 0 & 0 & 0 & 0 \\ 0 & -\frac{1}{\mu} & 0 & 0 & 0 & 0 \end{pmatrix}$$

The eigenvalues of A are $c = \pm \frac{1}{\epsilon\mu}$ (twice) and 0 (twice). Thus, two boundary conditions need to be imposed, two are determined from the interior and two are not clear. We shall see that we impose $\mathbf{E}_{\parallel} = 0$ (two conditions) and $\mathbf{H}_{\perp} = 0$ (one condition).

The structure of the paper is as follows: In Section 2 we introduce the background. In Section 3 we present our scheme, and Section 4 is devoted to stability analysis. Section 5 is devoted to numerical examples.

2. PRELIMINARIES

We consider a uniform discretization of $\Omega = [0, 1]^3$, $\Delta x = \Delta y = \Delta z = h$ and h_{τ} is the time-step. We introduce the following notations:

- $\mathbf{x} = (x, y, z) \in \mathbb{R}^3$.
- $r = \frac{h_{\tau}}{h}$ is the Courant-Friedrichs-Lewy (CFL) number.
- $\mathbf{E}(t, \mathbf{x}) = (E_x(t, \mathbf{x}), E_y(t, \mathbf{x}), E_z(t, \mathbf{x}))$, $\mathbf{H}(t, \mathbf{x}) = (H_x(t, \mathbf{x}), H_y(t, \mathbf{x}), H_z(t, \mathbf{x}))$.
- Δ denotes the Laplacian with respect to \mathbf{x} .
- $\Delta \mathbf{E} = (\Delta E_x, \Delta E_y, \Delta E_z)$, $\Delta \mathbf{H} = (\Delta H_x, \Delta H_y, \Delta H_z)$.
- \mathbf{E}^n (resp. $\mathbf{H}^{n+1/2}$) denotes $\mathbf{E}(t = nh_{\tau})$ (resp. $\mathbf{H}(t = (n + 1/2)h_{\tau})$).
- For $i, j, k \in \mathbb{N} \cup \{0\}$, $x_i = ih$, $y_j = jh$, $z_k = kh$.

- $x_{i+\frac{1}{2}} = (i + \frac{1}{2})h, y_{j+\frac{1}{2}} = (j + \frac{1}{2})h, z_{k+\frac{1}{2}} = (k + \frac{1}{2})h.$
- $[N] = \{0, 1, \dots, N\}, \quad N \in \mathbb{N}.$
- $[k, m] = \{k, k+1, \dots, m\}, \quad k < m \in \mathbb{N}.$
- $\mathbf{1}$ denotes the identity operator.
- For any operator $T : \mathbb{R}^M \rightarrow \mathbb{R}^N$, $\|T\| := \sup_{0 \neq x \in \mathbb{R}^N} \frac{|Tx|}{|x|}.$
- $\partial_\tau := \frac{\partial}{\partial \tau}$ and $\partial_\tau^2 := \frac{\partial^2}{\partial \tau^2}.$
- $\delta_\tau U^{n+\frac{1}{2}} := \frac{U^{n+1} - U^n}{h_\tau}.$

To discretize the equations, we introduce a staggered mesh in both space and time as in the Yee scheme [17]. With this arrangement, all space derivatives are spread over a single mesh width, and the central time and space derivatives are centered at the same point, similar to that of the Yee scheme. \mathbf{E} is evaluated at time nh_τ while \mathbf{H} and \mathbf{J} are evaluated at time $(n+\frac{1}{2})h_\tau$. For the spatial discretization, we define the following meshes:

$$\Omega_h^{E_z} := \{(x_i, y_j, z_{k+\frac{1}{2}}), \quad (i, j, k) \in [N]^2 \times [N-1]\} \quad (2.1)$$

$$\Omega_h^{E_y} := \{(x_i, y_{j+\frac{1}{2}}, z_k), \quad (i, j, k) \in [N] \times [N-1] \times [N]\}$$

$$\Omega_h^{E_x} := \{(x_{i+\frac{1}{2}}, y_j, z_k), \quad (i, j, k) \in [N-1] \times [N]^2\}$$

$$\Omega_h^{H_z} := \{(x_{i+\frac{1}{2}}, y_{j+\frac{1}{2}}, z_k), \quad (i, j, k) \in [N-1]^2 \times [N]\}$$

$$\Omega_h^{H_y} := \{(x_{i+\frac{1}{2}}, y_j, z_{k+\frac{1}{2}}), \quad (i, j, k) \in [N-1] \times [N] \times [N-1]\} \quad (2.2)$$

$$\Omega_h^{H_x} := \{(x_i, y_{j+\frac{1}{2}}, z_{k+\frac{1}{2}}), \quad (i, j, k) \in [N] \times [N-1]^2\}.$$

For each $s = x, y, z$ we define the interior meshes:

$$\text{int}(\Omega_h^{E_s}) := (0, 1)^3 \cap \Omega_h^{E_s}, \quad \text{int}(\Omega_h^{H_s}) := (0, 1)^3 \cap \Omega_h^{H_s}.$$

By convention, $x_0 = y_0 = z_0 = 0$ and $x_N = y_N = z_N = 1$. We denote

$$\Omega_h^{\mathbf{E}} := \Omega_h^{E_x} \times \Omega_h^{E_y} \times \Omega_h^{E_z}, \quad \Omega_h^{\mathbf{H}} := \Omega_h^{H_x} \times \Omega_h^{H_y} \times \Omega_h^{H_z},$$

and

$$\begin{aligned} \text{int}(\Omega_h^{\mathbf{E}}) &:= \text{int}(\Omega_h^{E_x}) \times \text{int}(\Omega_h^{E_y}) \times \text{int}(\Omega_h^{E_z}), & \partial\Omega_h^{\mathbf{E}} &:= \Omega_h^{\mathbf{E}} \setminus \text{int}(\Omega_h^{\mathbf{E}}) \\ \text{int}(\Omega_h^{\mathbf{H}}) &:= \text{int}(\Omega_h^{H_x}) \times \text{int}(\Omega_h^{H_y}) \times \text{int}(\Omega_h^{H_z}), & \partial\Omega_h^{\mathbf{H}} &:= \Omega_h^{\mathbf{H}} \setminus \text{int}(\Omega_h^{\mathbf{H}}) \end{aligned}$$

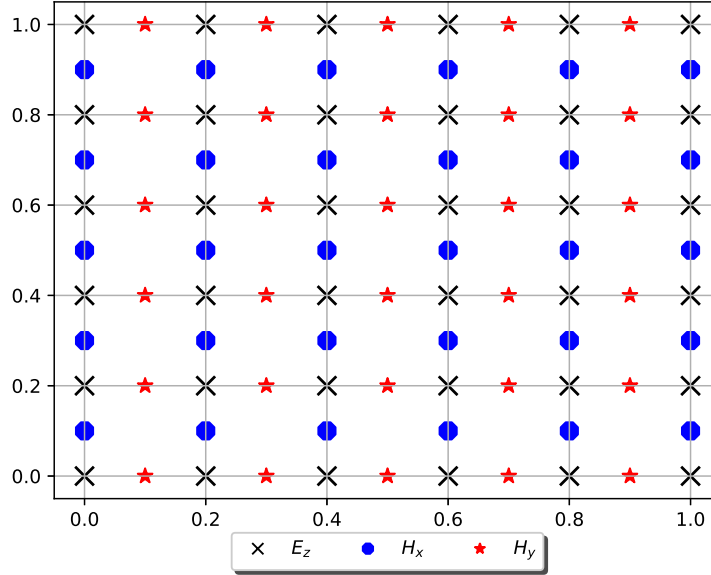


FIGURE 1. The grid points of $\Omega_h^{E_z}, \Omega_h^{H_x}, \Omega_h^{H_y}$ projected on the (x, y) plane in the case $N = 5$.

see Figure 1 for illustration of the sets $\Omega_h^{E_z}, \Omega_h^{H_x}, \Omega_h^{H_y}$ projected on the x, y plane. The discretized functions $\mathbf{E}_h, \mathbf{H}_h$ are then defined as:

$$\mathbf{E}_h^n := \mathbf{E}(nh_\tau, \Omega_h^{\mathbf{E}}), \quad \mathbf{H}_h^{n+\frac{1}{2}} := \mathbf{H}\left(\left(n + \frac{1}{2}\right)h_\tau, \Omega_h^{\mathbf{H}}\right).$$

With this arrangement, the boundary condition $\vec{n} \times \mathbf{E} = 0$ on $\partial\Omega_h^{\mathbf{E}}$ implies that

$$\begin{aligned} E_x(x_{i+\frac{1}{2}}, 0, z_j) &= E_x(x_{i+\frac{1}{2}}, N, z_j) = E_x(x_{i+\frac{1}{2}}, y_j, 0) = E_x(x_{i+\frac{1}{2}}, y_j, N) = 0, \\ E_y(0, y_{j+\frac{1}{2}}, z_j) &= E_y(N, y_{j+\frac{1}{2}}, z_j) = E_y(x_i, y_{j+\frac{1}{2}}, 0) = E_y(x_i, y_{j+\frac{1}{2}}, N) = 0, \\ E_z(0, y_j, z_{k+\frac{1}{2}}) &= E_x(N, y_j, z_{k+\frac{1}{2}}) = E_z(x_i, 0, z_{k+\frac{1}{2}}) = E_z(x_i, N, z_{k+\frac{1}{2}}) = 0. \end{aligned} \tag{2.3}$$

In short, $E_x = 0$ when $y = 0, 1$ and $z = 0, 1$; $E_y = 0$ when $x = 0, 1$ and $z = 0, 1$; $E_z = 0$ when $x = 0, 1$ and $y = 0, 1$.

2.1. Boundary conditions for time derivatives. We will now derive the boundary conditions for the time derivatives of the fields \mathbf{E} and \mathbf{H} rather than the fields themselves. We do so since time marching with our compact scheme derived in Section 3 involves solving elliptic equations for the time derivatives of the fields (see equation (3.1a) and (3.1b)).

By (2.3), we have the following Dirichlet-type boundary conditions:

$$\begin{aligned}\partial_\tau E_x &= 0 \text{ if } y=0, 1 \text{ and } z=0, 1, \\ \partial_\tau E_y &= 0 \text{ if } x=0, 1 \text{ and } z=0, 1, \\ \partial_\tau E_z &= 0 \text{ if } x=0, 1 \text{ and } y=0, 1.\end{aligned}\tag{2.4}$$

Moreover, differentiating the Gauss law of electricity $\nabla \cdot \mathbf{E} = \frac{\rho}{\varepsilon}$ with respect to time and using (2.3) we see that, for the remaining variables the Neumann-type conditions hold:

$$\begin{aligned}\partial_x \partial_\tau E_x &= \frac{\partial_\tau \rho}{\varepsilon} \text{ if } x = 0, 1, \\ \partial_y \partial_\tau E_y &= \frac{\partial_\tau \rho}{\varepsilon} \text{ if } y = 0, 1, \\ \partial_z \partial_\tau E_z &= \frac{\partial_\tau \rho}{\varepsilon} \text{ if } z = 0, 1.\end{aligned}$$

The Faraday law $\partial_\tau \mathbf{H} = -\frac{1}{Z} \nabla \times \mathbf{E}$ yields the following Dirichlet-type boundary conditions:

$$\begin{aligned}\partial_\tau H_x &= 0 \text{ if } x = 0, 1, \\ \partial_\tau H_y &= 0 \text{ if } y = 0, 1, \\ \partial_\tau H_z &= 0 \text{ if } z = 0, 1.\end{aligned}\tag{2.5}$$

In Table 1, we provide the values of the second-order derivatives at the boundaries of Ω that we need for subsequent analysis and that can be derived from equations (2.4) and (2.5) by differentiation.

	$x = 0, 1$	$y = 0, 1$	$z = 0, 1$
$\partial_\tau^2 E_x$	-	0	0
$\partial_\tau^2 E_y$	0	-	0
$\partial_\tau^2 E_z$	0	0	-
$\partial_\tau \partial_y H_z$	-	-	0
$\partial_\tau \partial_z H_y$	-	0	-
$\partial_\tau \partial_z H_x$	0	-	-
$\partial_\tau \partial_x H_z$	-	-	0
$\partial_\tau \partial_x H_y$	-	0	-
$\partial_\tau \partial_y H_x$	0	-	-

TABLE 1. Second-order derivatives in time and mixed space-time derivatives at the boundaries of Ω . The first three rows follow from (2.4). The other six rows are an implication of (2.5).

The Ampère law $\partial_\tau \mathbf{E} = Z(\nabla \times \mathbf{H} - \mathbf{J})$ implies that

$$\begin{aligned}\partial_\tau^2 E_x &= Z \left(\frac{\partial H_z}{\partial_y \partial \tau} - \frac{\partial^2 H_y}{\partial_z \partial \tau} - \partial_\tau \mathbf{J}_x \right), \\ \partial_\tau^2 E_y &= Z \left(\frac{\partial H_x}{\partial_z \partial \tau} - \frac{\partial^2 H_z}{\partial_x \partial \tau} - \partial_\tau \mathbf{J}_y \right), \\ \partial_\tau^2 E_z &= Z \left(\frac{\partial H_y}{\partial_x \partial \tau} - \frac{\partial^2 H_x}{\partial_y \partial \tau} - \partial_\tau \mathbf{J}_z \right).\end{aligned}$$

Substituting the values from Table 1 into these equations, we obtain the following six Neumann-type boundary conditions:

$$\begin{aligned}\partial_y \partial_\tau H_x &= -\partial_\tau \mathbf{J}_z \text{ if } y = 0, 1 & \partial_z \partial_\tau H_x &= \partial_\tau \mathbf{J}_y \text{ if } z = 0, 1, \\ \partial_x \partial_\tau H_y &= \partial_\tau \mathbf{J}_z \text{ if } x = 0, 1 & \partial_z \partial_\tau H_y &= -\partial_\tau \mathbf{J}_x \text{ if } z = 0, 1, \\ \partial_x \partial_\tau H_z &= -\partial_\tau \mathbf{J}_y \text{ if } x = 0, 1 & \partial_y \partial_\tau H_z &= \partial_\tau \mathbf{J}_x \text{ if } y = 0, 1.\end{aligned}$$

With these arrangements, the derivatives $\partial_\tau \mathbf{E}$ and $\partial_\tau \mathbf{H}$ are supplied with well-defined boundary conditions, as summarized in Table 2. In short, on $\partial\Omega$ we have $\partial_\tau \mathbf{E}_\parallel = \partial_\tau \mathbf{H}_\perp = 0$, while $\partial_\tau \mathbf{E}_\perp$ and $\partial_\tau \mathbf{H}_\parallel$ obey a Neumann condition. As discussed earlier, Dirichlet conditions are true boundary conditions while Neumann conditions are derived from the interior equations.

	$x = 0, 1$	$y = 0, 1$	$z = 0, 1$
$\partial_\tau E_x$	Neumann	Dirichlet	Dirichlet
$\partial_\tau E_y$	Dirichlet	Neumann	Dirichlet
$\partial_\tau E_z$	Dirichlet	Dirichlet	Neumann
$\partial_\tau H_x$	Dirichlet	Neumann	Neumann
$\partial_\tau H_y$	Neumann	Dirichlet	Neumann
$\partial_\tau H_z$	Neumann	Neumann	Dirichlet

TABLE 2. Boundary conditions for the time derivatives of the Cartesian components of \mathbf{E} and \mathbf{H} .

3. THE SCHEME

3.1. Equation based derivation. We now extend the second-order accurate Yee scheme to a fourth-order accurate scheme, in both space and time, while maintaining the compact Yee stencil. The idea is to use a Taylor expansion in time to the next order and then replace the resulting third-order time derivatives by space derivatives using Maxwell's equations.

The fourth-order Taylor expansion applied to (1.2) and combined with equations (1.3) and (1.4) yields:

$$\begin{aligned} Z(\nabla \times \mathbf{H}^{n+1/2} - \mathbf{J}^{n+1/2}) &= \left(\frac{\partial \mathbf{E}}{\partial \tau} \right)^{n+1/2} = \frac{\mathbf{E}^{n+1} - \mathbf{E}^n}{h_\tau} - \frac{h_\tau^2}{24} \frac{\partial^3 \mathbf{E}^{n+1/2}}{\partial \tau^3} + O(h_\tau^4) = \\ \delta_\tau \mathbf{E}^{n+1/2} - \frac{h_\tau^2}{24} \partial_\tau (-Z \partial_\tau \mathbf{J}^{n+1/2} - \nabla(\nabla \cdot \mathbf{E}^{n+1/2}) + \Delta \mathbf{E}^{n+1/2}) + O(h_\tau^4) &= \\ \delta_\tau \mathbf{E}^{n+1/2} - \frac{h_\tau^2}{24} (-Z \partial_\tau^2 \mathbf{J}^{n+1/2} - \nabla(\nabla \cdot \partial_\tau \mathbf{E}^{n+1/2}) + \Delta \partial_\tau \mathbf{E}^{n+1/2}) + O(h_\tau^4) &= \\ \delta_\tau \mathbf{E}^{n+1/2} - \frac{h_\tau^2}{24} (-Z \partial_\tau^2 \mathbf{J}^{n+1/2} + Z \nabla(\nabla \cdot \mathbf{J}^{n+1/2}) + \Delta \partial_\tau \mathbf{E}^{n+1/2}) + O(h_\tau^4). \end{aligned}$$

Since $\Delta \partial_\tau \mathbf{E}^{n+1/2} = \Delta \delta_\tau \mathbf{E}^{n+1/2} + O(h_\tau^2)$, we have that

$$\begin{aligned} Z(\nabla \times \mathbf{H}^{n+1/2} - \mathbf{J}^{n+1/2}) &= \\ \delta_\tau \mathbf{E}^{n+1/2} - \frac{h_\tau^2}{24} (-Z \partial_\tau^2 \mathbf{J}^{n+1/2} + Z \nabla(\nabla \cdot \mathbf{J}^{n+1/2}) + \Delta \delta_\tau \mathbf{E}^{n+1/2}) + O(h_\tau^4). \end{aligned}$$

Similarly, we have for \mathbf{H} :

$$\begin{aligned} -\frac{1}{Z} \nabla \times \mathbf{E}^{n+1} &= \frac{\partial \mathbf{H}^{n+1}}{\partial \tau} = \\ \delta_\tau \mathbf{H}^{n+1} - \frac{h_\tau^2}{24} \partial_\tau (\Delta \mathbf{H}^{n+1} - \nabla \times \partial_\tau \mathbf{J}^{n+1}) + O(h_\tau^4) &= \\ \delta_\tau \mathbf{H}^{n+1} - \frac{h_\tau^2}{24} (\delta_\tau \Delta \mathbf{H}^{n+1} - \nabla \times \partial_\tau^2 \mathbf{J}^{n+1}) + O(h_\tau^4). \end{aligned}$$

Thus, at each time step we obtain several uncoupled modified Helmholtz equations which are positive definite. Note, that for more complicated situations the equations might be coupled at the boundary.

$$-\Delta \delta_\tau \mathbf{E}^{n+\frac{1}{2}} + \frac{24}{h_\tau^2} \delta_\tau \mathbf{E}^{n+\frac{1}{2}} = Z \frac{24}{h_\tau^2} \nabla \times \mathbf{H}^{n+\frac{1}{2}} + P(\mathbf{J})^{n+\frac{1}{2}} + O(h_\tau^4 + h^4) \quad \text{in } (0, 1)^3, \quad (3.1a)$$

$$-\Delta \delta_\tau \mathbf{H}^{n+1} + \frac{24}{h_\tau^2} \delta_\tau \mathbf{H}^{n+1} = -\frac{1}{Z} \frac{24}{h_\tau^2} \nabla \times \mathbf{E}^{n+1} - \nabla \times \partial_\tau^2 \mathbf{J}^{n+1} + O(h_\tau^4 + h^4) \quad \text{in } (0, 1)^3, \quad (3.1b)$$

where

$$P(\mathbf{J})^{n+\frac{1}{2}} \stackrel{\text{def}}{=} Z \left(-\mathbf{J}^{n+\frac{1}{2}} - \nabla(\nabla \cdot \mathbf{J}^{n+\frac{1}{2}}) + \frac{\partial^2 \mathbf{J}^{n+\frac{1}{2}}}{\partial \tau^2} \right). \quad (3.2)$$

Equations (3.1) are supplemented by the boundary conditions for the functions $\delta_\tau \mathbf{E}$ and $\delta_\tau \mathbf{H}$, as discussed in Section 2.

3.2. Modified Helmholtz equation. In a Cartesian coordinate system, each of the equations (3.1a) and (3.1b) gets split into three scalar modified Helmholtz equations:

$$-\Delta\phi + \kappa^2\phi = \kappa^2F, \quad \kappa^2 > 0. \quad (3.3)$$

We use the fourth-order accurate compact finite-difference scheme [14] for solving elliptic equations of the type (3.3).

Consider an equally-spaced mesh of dimension $N_x \times N_y \times N_z$ and size h in each direction. We denote by D_{xx} , D_{yy} , and D_{zz} the standard second-order central-difference operators and define

$$\Delta_h \stackrel{\text{def}}{=} D_{xx} + D_{yy} + D_{zz}, \quad \Upsilon_h \stackrel{\text{def}}{=} D_{zz}D_{xx} + D_{yy}D_{zz} + D_{xx}D_{yy}.$$

Then, the fourth-order accurate scheme for (3.3) is given by [14]:

$$-\left(\Delta_h + \frac{h^2}{6}\Upsilon_h\right)\phi + \kappa^2\left(1 + \frac{\kappa^2h^2}{12}\right)\phi = \kappa^2\left(1 + \frac{\kappa^2h^2}{12} + \frac{h^2}{12}\Delta_h\right)F. \quad (3.4)$$

If ΔF is known at the grid nodes to fourth-order accuracy, then (3.3) can be simplified further to

$$-\left(\Delta_h + \frac{h^2}{6}\Upsilon_h\right)\phi + \kappa^2\left(1 + \frac{\kappa^2h^2}{12}\right)\phi = \kappa^2\left(1 + \frac{\kappa^2h^2}{12}\right)F + \frac{\kappa^2h^2}{12}\Delta F. \quad (3.5)$$

Letting $\kappa^2 = \frac{24}{h_\tau^2}$ in (3.1) and (3.4) gives rise to six elliptic equations of type (3.3) with ϕ and F specified in Table 3. Once the discretization in space has been applied (Section 3.4), equations (3.1) lead to six positive definite linear systems to be solved independently by conjugate gradients. Note that, it is difficult to use multigrid since the grid dimension for different various equations is not the same and hence not all equations can have 2^n grid nodes in every direction.

Eq.	ϕ	F
1	$\delta_\tau E_x^{n+\frac{1}{2}}$	$Z(\partial_y H_z^{n+\frac{1}{2}} - \partial_z H_y^{n+\frac{1}{2}}) + \frac{h_\tau^2}{24}P(\mathbf{J}^{n+\frac{1}{2}})_x$
2	$\delta_\tau E_y^{n+\frac{1}{2}}$	$Z(\partial_z H_x^{n+\frac{1}{2}} - \partial_x H_z^{n+\frac{1}{2}}) + \frac{h_\tau^2}{24}P(\mathbf{J}^{n+\frac{1}{2}})_y$
3	$\delta_\tau E_z^{n+\frac{1}{2}}$	$Z(\partial_x H_y^{n+\frac{1}{2}} - \partial_y H_x^{n+\frac{1}{2}}) + \frac{h_\tau^2}{24}P(\mathbf{J}^{n+\frac{1}{2}})_z$
4	$\delta_\tau H_x^{n+\frac{3}{2}}$	$-\frac{1}{Z}(\partial_y E_z^{n+1} - \partial_z E_y^{n+1}) - \frac{h_\tau^2}{24}(\nabla \times \partial_\tau^2 \mathbf{J}^{n+1})_x$
5	$\delta_\tau H_y^{n+\frac{3}{2}}$	$-\frac{1}{Z}(\partial_z E_x^{n+1} - \partial_x E_z^{n+1}) - \frac{h_\tau^2}{24}(\nabla \times \partial_\tau^2 \mathbf{J}^{n+1})_y$
6	$\delta_\tau H_z^{n+\frac{3}{2}}$	$-\frac{1}{Z}(\partial_x E_y^{n+1} - \partial_y E_x^{n+1}) - \frac{h_\tau^2}{24}(\nabla \times \partial_\tau^2 \mathbf{J}^{n+1})_z$

TABLE 3. The expressions for ϕ and F in (3.3) ($P(\mathbf{J})$ is given by (3.2)).

3.3. Neumann boundary conditions. We reemphasize that Neumann conditions for a first-order system are not imposed boundary conditions. They are rather an implication of the PDEs in the interior. Let $\Omega = [0, 1]^3$. We define ghost nodes outside the numerical grid so that the Neumann conditions are satisfied to fourth-order accuracy (see Figure 2).

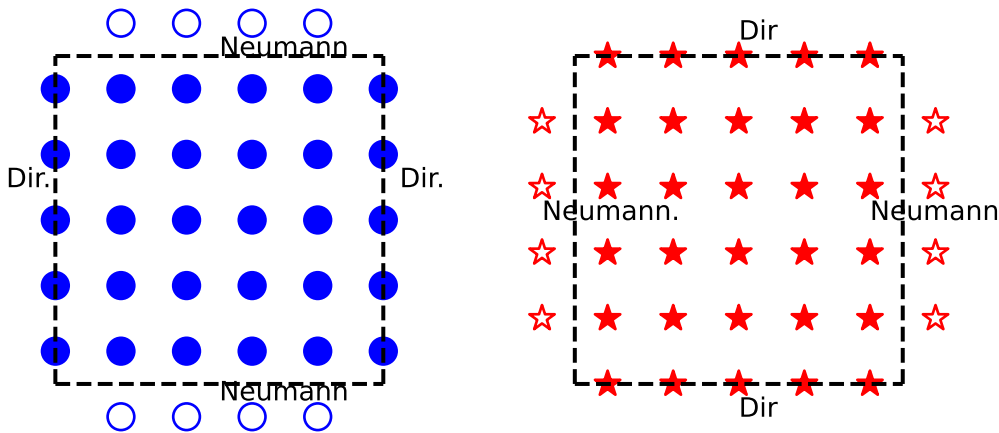


FIGURE 2. Left: The grid nodes for H_x projected onto the (x, y) plane in the case $N_x = N_y = 5$. The unit square is bounded by the dashed line. Solid circles show the mesh points of $\Omega_h^{H_x}$. Hollow circles denote the ghost points induced by the Neumann boundary conditions at $y = 0, 1$. Right: The grid nodes for H_y projected onto the (x, y) plane in the case $N_x = N_y = 5$. The unit square is bounded by the dashed frame. Solid stars show the mesh points of $\Omega_h^{H_y}$. Hollow stars denote ghost points induced by the Neumann boundary conditions at $x = 0, 1$.

We propose two methods for the implementation of the Neumann boundary conditions. *Method 1 (equation based).* Consider, without loss of generality, equation (3.3) with the Neumann boundary condition $\partial_x \phi(0, y, z) = g(y, z)$. Differentiating (3.3) with respect to x (cf. [14]), we have:

$$\phi_x(0, x, z) = \frac{\phi(\frac{1}{2}h, y, z) - \phi(-\frac{1}{2}h, y, z)}{h} + \frac{h^2}{24} (\phi_{xyy} + \phi_{xzz} - \kappa^2 \phi_x - \kappa^2 F_x) + O(h^4). \quad (3.6)$$

Assume that $\phi_{xyy} + \phi_{xzz}$ is known for $x = 0$. Setting $x = 0$ in (3.6), we define the ghost value $\phi(-\frac{1}{2}h, y, z)$ such that the Neumann boundary condition $\partial_x \phi = g(y, z)$ is satisfied to fourth-order.

Method 2 (Taylor based). By Taylor's expansion

$$\phi_x(0, y, z) = \frac{\phi(\frac{1}{2}h, y, z) - \phi(-\frac{1}{2}h, y, z)}{h} - \frac{h^2}{24} \partial_{xxx} \phi(0, y, z) + O(h^4). \quad (3.7)$$

Hence, knowing $\partial_x \phi$ and $\partial_{xxx} \phi$ at $x=0$ enables one to obtain the ghost variable $\phi(-\frac{1}{2}h, y, z)$ using (3.7).

Next, we show how to approximate the Neumann-type boundary conditions to fourth-order accuracy for $\partial_\tau \mathbf{E}$ using Method 1 and for $\partial_\tau \mathbf{H}$ using Method 2.

Lemma 3.1. *Let $\phi(x, y, z) = \partial_\tau E_x$ be evaluated at some fixed τ_0 . Then, the quantities*

$$\phi_{xyy}(0, y, z), \phi_{xzz}(0, y, z), \phi_x(0, y, z), \text{ and } F_x$$

are known to fourth-order accuracy. (Recall that, F contains the terms involving only $\partial_z H_y - \partial_y H_z$ and \mathbf{J} .) If, in addition, $\mathbf{J} = 0$ and $\rho = 0$, then $\phi_{xyy}(0, y, z) = \phi_{xzz}(0, y, z) = \phi_x(0, y, z) = F_x(0, y, z) = 0$.

Proof. $\phi_x(0, y, z)$ equals to $\partial_\tau E_x$ at $x = 0$, which has already been specified. Moreover, we have

$$\partial_x E_x + \partial_y E_y + \partial_z E_z = \frac{\rho}{\varepsilon}. \quad (3.8)$$

Differentiating (3.8) twice with respect to y and once with respect to τ , we arrive at

$$-\partial_{xyy} \phi + \partial_{\tau yy}(\rho/\varepsilon) = \partial_{yyy} \phi + \partial_{zyy} \phi.$$

If $x = 0$, then $\partial_{\tau yyy} E_x = \partial_{\tau zyy} E_x = 0$, and hence if $x = 0$, then $\partial_{xyy} \phi = \partial_{\tau yy}(\rho/\varepsilon)$. Differentiating (3.8) twice with respect to z and once with respect to τ , we get

$$-\partial_{xzz} \phi + \partial_{\tau zz}(\rho/\varepsilon) = \partial_{yzz} \phi + \partial_{zzz} \phi.$$

If $x = 0$, then $\partial_{\tau zzz} E_x = \partial_{\tau yzz} E_x = 0$, and hence at $x = 0$ we have $\partial_{xzz} \phi = \partial_{\tau zz}(\rho/\varepsilon)$.

To obtain F_x at $x = 0$, it is sufficient to evaluate $\partial_x(\partial_z H_y - \partial_y H_z)$. This quantity, in turn, can be derived via the Ampère law $\partial_\tau \mathbf{E} = Z(\nabla \times \mathbf{H} - \mathbf{J})$ if $\partial_{x\tau} E_x$ is available. And the latter is known through the Neumann boundary condition for $\partial_\tau \mathbf{E}$ at $x = 0$.

The second assertion follows immediately by virtue of the same argument. \square

By repeating the previous proof for the remaining faces of the cube $\Omega = [0, 1]^3$ and field components E_y and E_z , we obtain the following

Corollary 3.2. *Neumann boundary conditions for equation (3.1a) admit a compact fourth-order accurate discretization by means of Method 1.*

Next, we will show how one can use Method 2 to build a compact discretization of the Neumann boundary conditions for $\partial_\tau \mathbf{H}$.

Lemma 3.3. *Let $\phi(x, y, z) = \partial_\tau H_y$ be evaluated at some fixed τ_0 . Then, the term ϕ_{xxx} at $x = 0, 1$ can be approximated to fourth-order accuracy.*

Proof. Assume without loss of generality that $Z = 1$. The equation

$$\partial_\tau E_z = \partial_x H_y - \partial_y H_x - \mathbf{J}_z \quad (3.9)$$

(cf. (1.2a)) and boundary conditions $\partial_\tau E_z = 0$ at $x = 0, 1$ imply that at $x = 0, 1$

$$\partial_{\tau xxx} H_y = \partial_{\tau yxx} H_x + \partial_{\tau xx} \mathbf{J}_z.$$

Then, we use $\partial_\tau \nabla \cdot \mathbf{H} = 0$ and replace $\partial_x H_x$ with $-\partial_{\tau y} H_y - \partial_{\tau z} H_z$. This yields:

$$\partial_{\tau yxx} H_x = -\partial_{\tau yyx} H_y - \partial_{\tau xyz} H_z.$$

To complete the proof, we have to approximate $\partial_{\tau yyx} H_y$ and $\partial_{\tau xyz} H_z$. This is done as follows. We use (3.9) again to obtain

$$\partial_{\tau yyx} H_y = \partial_{\tau yyy} H_x + \partial_{\tau yy} \mathbf{J}_z.$$

At $x = 0, 1$, the first equation of (2.5) implies that $\partial_{\tau yyy} H_x = 0$.

To approximate $\partial_{\tau xyz} H_z$, we use the y -component of the Ampère law (1.2a):

$$\partial_\tau E_y = \partial_z H_x - \partial_x H_z - \mathbf{J}_y.$$

Therefore, at $x = 0, 1$ we have:

$$\partial_x H_z = \mathbf{J}_y + \partial_z H_x$$

and

$$\partial_{\tau xyz} H_z = \partial_{\tau yz} \mathbf{J}_y + \partial_{\tau yzz} H_x.$$

Since $\partial_\tau H_x = 0$ at $x = 0, 1$, we finally derive:

$$\partial_{\tau yzz} H_x = 0.$$

This completes the proof. \square

By repeating the previous procedure for H_x and H_z , we obtain the following corollaries.

Corollary 3.4. *Neumann boundary conditions for equation (3.1b) admit a compact fourth-order accurate discretization by means of Method 2.*

Corollary 3.5. *Assume that $\rho = 0$ and $\mathbf{J} = 0$. Then, all Neumann boundary conditions obtained for $\partial_\tau \mathbf{E}$ and $\partial_\tau \mathbf{H}$ are homogeneous and all the derivatives in (3.6), (3.7) vanish. In particular, $\phi(\tilde{x} - \frac{1}{2}) = \phi(\tilde{x} + \frac{1}{2})$ is a fourth-order accurate approximation to the homogeneous Neumann condition at the boundary point \tilde{x} (see also Section 5).*

We emphasize that, the right hand side, F , needs to be approximated with fourth-order accuracy. This is done using a fourth-order Padé approximation for the curl operator (see details in Appendix A.1). Then, we solve equations 1, 2, and 3 from Table 3 using the scheme (3.4), and subsequently solve equations 4, 5, and 6 from Table 3 using the scheme (3.5).

In view of equations (3.4) and (3.5), we also define the following operators.

Definition 3.6. *For any $s = x, y, z$ and $G = H_s, E_s$, let*

$$P_1^G, P_2^G : \text{int}(\Omega_h)^G \rightarrow \text{int}(\Omega_h)^G$$

be the symmetric operators given by

$$P_1^G := - \left(\Delta_h + \frac{h^2}{6} \mathcal{I}_h \right) + \frac{24}{h_\tau^2} \left(1 + \frac{2}{r^2} \right),$$

$$P_2^G := \frac{24}{h_\tau^2} \left(-1 - \frac{2}{r^2} - \frac{h^2}{12} \Delta_h \right).$$

We omit the superscript G whenever it does not lead to any ambiguity.

Hereafter, $r = \frac{h_\tau}{h}$ will denote the CFL number. As shown in Appendix A.2, if $r < \sqrt{3 + \sqrt{21}}$, then P_2^G and P_1^G are symmetric positive definite matrices and the following estimates hold:

$$0 < \frac{2}{r^2} \leq \left\| \frac{h_\tau^2}{24} P_2^G \right\| \leq 1 + \frac{2}{r^2}, \quad (3.10)$$

$$1 < 1 + \frac{2}{r^2} - \frac{r^2}{6} \leq \left\| \frac{h_\tau^2}{24} P_1^G \right\| \leq 1 + \frac{2}{r^2} + \frac{r^2}{2}. \quad (3.11)$$

In particular,

$$\left\| (P_1^G)^{-1} P_2^G \right\| \geq \frac{\frac{2}{r^2}}{1 + \frac{2}{r^2} + \frac{r^2}{2}}.$$

3.4. The numerical scheme. Let

$$\mathbf{curl}_h \stackrel{\text{def}}{=} \begin{pmatrix} 0 & -\delta_z & \delta_y \\ \delta_z & 0 & -\delta_x \\ -\delta_y & \delta_x & 0 \end{pmatrix}$$

be the block matrix representing a spatial Padé fourth-order finite-difference approximation of the curl operator. See Appendix A.1 for the full definition of the matrix \mathbf{curl}_h .

Let \mathbf{E}_h^n and $\Delta \mathbf{E}_h^n$ be given on $\Omega_h^{\mathbf{E}}$ and let $\mathbf{H}_h^{n+\frac{1}{2}}$ be given on $\Omega_h^{\mathbf{H}}$. To advance in time, we take two steps.

Step 1:

$$\mathbf{E}_h^{n+1} = \begin{pmatrix} E_x^n + h_\tau E_x^* \\ E_y^n + h_\tau E_y^* \\ E_y^n + h_\tau E_y^* \end{pmatrix}$$

where

$$\underbrace{\begin{pmatrix} P_1^{E_x} & 0 & 0 \\ 0 & P_1^{E_y} & \\ 0 & 0 & P_1^{E_z} \end{pmatrix}}_{P_1^{\mathbf{E}}} \begin{pmatrix} E_x^* \\ E_y^* \\ E_z^* \end{pmatrix} = ZP(\mathbf{J}^{n+1/2}) + \kappa^2 Z \begin{pmatrix} 0 & -\delta_z & \delta_y \\ \delta_z & 0 & -\delta_x \\ -\delta_y & \delta_x & 0 \end{pmatrix} \left[\left(1 + \frac{\kappa^2 h^2}{12}\right) \begin{pmatrix} H_x^{n+1/2} \\ H_y^{n+1/2} \\ H_z^{n+1/2} \end{pmatrix} + \frac{h^2}{12} \begin{pmatrix} \Delta_h H_x^{n+1/2} \\ \Delta_h H_y^{n+1/2} \\ \Delta_h H_z^{n+1/2} \end{pmatrix} \right]$$

(cf. Section 3.2). Extend \mathbf{E}_h^{n+1} to $\Omega_h^{\mathbf{E}}$ using the boundary conditions. Define

$$\Delta \mathbf{E}_h^{n+1} = \Delta \mathbf{E}_h^n + \kappa^2 (\mathbf{E}_h^{n+1} - \mathbf{E}_h^n) - Z \frac{24}{h_\tau} \begin{pmatrix} 0 & -\delta_z & \delta_y \\ \delta_z & 0 & -\delta_x \\ -\delta_y & \delta_x & 0 \end{pmatrix} \begin{pmatrix} H_x^{n+1/2} \\ H_y^{n+1/2} \\ H_z^{n+1/2} \end{pmatrix} - h_\tau P(\mathbf{J})^{n+1/2}$$

on $\Omega_h^{\mathbf{E}}$ (see (3.1))

Step 2:

$$\mathbf{H}_h^{n+3/2} = \begin{pmatrix} H_x^{n+1/2} + h_\tau H_x^* \\ H_y^{n+1/2} + h_\tau H_y^* \\ H_z^{n+1/2} + h_\tau H_z^* \end{pmatrix}$$

where

$$\underbrace{\begin{pmatrix} P_1^{H_x} & 0 & 0 \\ 0 & P_1^{H_y} & \\ 0 & 0 & P_1^{H_z} \end{pmatrix}}_{P_1^{\mathbf{H}}} \begin{pmatrix} H_x^* \\ H_y^* \\ H_z^* \end{pmatrix} - \frac{1}{Z} \nabla \times \partial_\tau^2 \mathbf{J}^{n+1} = -\frac{\kappa^2}{Z} \begin{pmatrix} 0 & -\delta_z & \delta_y \\ \delta_z & 0 & -\delta_x \\ -\delta_y & \delta_x & 0 \end{pmatrix} \left[\left(1 + \frac{\kappa^2 h^2}{12}\right) \begin{pmatrix} E_x^{n+1} \\ E_y^{n+1} \\ E_z^{n+1} \end{pmatrix} + \frac{h^2}{12} \begin{pmatrix} \Delta E_x^{n+1} \\ \Delta E_y^{n+1} \\ \Delta E_z^{n+1} \end{pmatrix} \right],$$

(cf. Section 3.2). Extend $\mathbf{H}_h^{n+3/2}$ to $\Omega_h^{\mathbf{H}}$ using the appropriate boundary condition.

4. STABILITY ANALYSIS

We assume, with no loss of generality, that $\rho = 0$, $\mathbf{J} = 0$, and $Z = 1$. The scheme can therefore be written in a compact way:

$$\mathbf{E}_h^{n+1} - \mathbf{E}_h^n = h_\tau P_1^{-1} \mathbf{curl}_h \left(\kappa^2 \left(1 + \frac{\kappa^2 h^2}{12} \right) \mathbf{H}_h^{n+1/2} + \frac{\kappa^2 h^2}{12} \Delta \mathbf{H}_h^{n+1/2} \right), \quad (4.1a)$$

$$\mathbf{H}_h^{n+3/2} - \mathbf{H}_h^{n+1/2} = -h_\tau P_1^{-1} \mathbf{curl}_h \left(\kappa^2 \left(1 + \frac{\kappa^2 h^2}{12} \right) \mathbf{E}_h^{n+1} + \frac{\kappa^2 h^2}{12} \Delta \mathbf{E}_h^{n+1} \right). \quad (4.1b)$$

We approximate Δ in equations (4.1a) and (4.1b) using the standard second-order difference Laplacian Δ_h (same as in (3.4)). Then, we recast (4.1a), (4.1b) as:

$$\begin{aligned} & \left(\mathbf{1} - \mathbf{h}_\tau \begin{pmatrix} 0 & 0 \\ -P_1^{-1} P_2 \mathbf{curl}_h & 0 \end{pmatrix} \right) \begin{pmatrix} \mathbf{E}^{n+1} \\ \mathbf{H}^{n+3/2} \end{pmatrix} = \\ & \left(\mathbf{1} - \mathbf{h}_\tau \begin{pmatrix} 0 & -P_1^{-1} P_2 \mathbf{curl}_h \\ 0 & 0 \end{pmatrix} \right) \begin{pmatrix} \mathbf{E}^n \\ \mathbf{H}^{n+1/2} \end{pmatrix}, \end{aligned} \quad (4.2)$$

where the operators P_1 and P_2 are introduced in Definition 3.6. Next, assume the solution is in the form of a plane wave:

$$\begin{pmatrix} \mathbf{E}^n \\ \mathbf{H}^{n+1/2} \end{pmatrix}_{i,j,k} = \sigma^n (\exp(-\sqrt{-1}(\xi_x i h + \xi_y j h + \xi_z k h))) \begin{pmatrix} \mathbf{E}_0 \\ \mathbf{H}_0 \end{pmatrix}.$$

Let $Q = -P_1^{-1} P_2 \mathbf{curl}_h$ and let λ denote an eigenvalue of Q . We substitute the plane wave solution into (4.2) and derive

$$\begin{pmatrix} \sigma - 1 & \lambda h_\tau \\ -\sigma h_\tau \lambda & \sigma - 1 \end{pmatrix} \begin{pmatrix} \mathbf{E}_0 \\ \mathbf{H}_0 \end{pmatrix} = \begin{pmatrix} 0 \\ 0 \end{pmatrix}.$$

Therefore,

$$\sigma^2 - \sigma(2 - \lambda^2 h_\tau^2) + 1 = 0.$$

In particular, $|h_\tau \lambda| \leq 2$ implies that $|\sigma| \leq 1$. Then, using the definition of the matrix A given by equation (A.2) and Remark A.1 (see Appendix A.1), we can derive the stability condition in the following form:

$$r 2\sqrt{3} \|A^{-1}\| \| -P_1^{-1} P_2 \| \leq 2 \Leftrightarrow r \leq \frac{1}{\sqrt{3} \|A^{-1}\| \cdot \| -P_1^{-1} P_2 \|}. \quad (4.3)$$

By (3.10), $r < \sqrt{3 + \sqrt{21}}$ implies that $\| -P_1^{-1} P_2 \| \geq \frac{\frac{2}{r^2}}{1 + \frac{2}{r^2} + \frac{r^2}{2}}$ (see Appendix A.2 for detail).

Therefore, the scheme is stable provided that

$$r \leq \min \left\{ \sqrt{3 + \sqrt{21}}, \frac{1 + \frac{2}{r^2} + \frac{r^2}{2}}{\sqrt{3} \|A^{-1}\| \frac{2}{r^2}} \right\}.$$

The inequality

$$\frac{1 + \frac{2}{r^2} + \frac{r^2}{2}}{\frac{2}{r^2}} \geq 1, \quad r \in (0, \infty)$$

gives rise to a sufficient stability condition

$$0 < r \leq \frac{1}{\sqrt{3}\|A^{-1}\|} \sim \frac{5}{6\sqrt{3}}. \quad (4.4)$$

In the following section we will examine a two-dimensional reduction of Maxwell's equation. A modification of Remark A.1 readily implies the stability condition

$$0 < r \leq \frac{1}{\sqrt{3}\|A^{-1}\|} \sim \frac{5}{6\sqrt{2}} \quad (4.5)$$

(cf. [18]). The numerical results summarized in Table 5 corroborate the stability estimate (4.5).

5. EXAMPLE: TRANSVERSE MAGNETIC WAVES IN $[0, 1]^2$

5.1. Numerical simulations data. For the computations, we consider the scaled two-dimensional TM system without any current or charges. Thus, the equations reduce to

$$\frac{\partial E_z}{\partial \tau} = Z \left(-\frac{\partial H_x}{\partial y} + \frac{\partial H_y}{\partial x} \right), \quad (5.1a)$$

$$\frac{\partial H_x}{\partial \tau} = -\frac{1}{Z} \frac{\partial E_z}{\partial y}, \quad (5.1b)$$

$$\frac{\partial H_y}{\partial \tau} = \frac{1}{Z} \frac{\partial E_z}{\partial x}. \quad (5.1c)$$

Since \mathbf{H} is given at time moments $n + 1/2$ we need to specify its initial condition at the time $t = \frac{\Delta\tau}{2}$. By Taylor series,

$$\mathbf{H} \left(\frac{h_\tau}{2} \right) = \mathbf{H}(0) + \left(\frac{h_\tau}{2} \right) \mathbf{H}_\tau(0) + \frac{1}{2} \left(\frac{h_\tau}{2} \right)^2 \mathbf{H}_{\tau\tau}(0) + \frac{1}{6} \left(\frac{h_\tau}{2} \right)^3 \mathbf{H}_{\tau\tau\tau}(0) + \frac{1}{24} \left(\frac{h_\tau}{2} \right)^4 \mathbf{H}_{\tau\tau\tau\tau}(0). \quad (5.2)$$

$\mathbf{H}_\tau(0)$ is given by (1.2b) and $\mathbf{H}_{\tau\tau}(0)$ is given by (1.4). Differentiating (1.4) yields:

$$\frac{\partial^3 \mathbf{H}}{\partial \tau^3} = -\nabla \times \nabla \times \mathbf{H}_\tau - \nabla \times \partial_{\tau\tau} \mathbf{J} = \Delta \mathbf{H}_\tau - \nabla \times \partial_{\tau\tau} \mathbf{J},$$

where, again, \mathbf{H}_τ is given by (1.2b). Similarly,

$$\frac{\partial^4 \mathbf{H}}{\partial \tau^4} = -\nabla \times \nabla \times \mathbf{H}_{\tau\tau} - \nabla \times \partial_{\tau^3} \mathbf{J} = \Delta \mathbf{H}_{\tau\tau} - \nabla \times \partial_{\tau\tau\tau} \mathbf{J},$$

where $\mathbf{H}_{\tau\tau}$ is given by (1.4). At the nodes on or next to a boundary, we have either Dirichlet or Neumann conditions as given in Table 2. For (5.1), we have assumed $\mathbf{J} = 0$. For the computations, we further assume $Z = 1$.

Let $k_x, k_y \in \mathbb{N}$ and let $\omega := Z\pi\sqrt{k_x^2 + k_y^2}$. We consider the analytical solutions

$$E_z(x, y) = \cos(\omega\tau) \sin(Z\pi k_x x) \sin(Z\pi k_y y), \quad (5.3a)$$

$$H_x(x, y) = -\frac{\sin(\omega\tau)}{\omega} \pi k_y \sin(Z\pi k_x x) \cos(Z\pi k_y y), \quad (5.3b)$$

$$H_y(x, y) = \frac{\sin(\omega\tau)}{\omega} \pi k_x \cos(Z\pi k_x x) \sin(Z\pi k_y y). \quad (5.3c)$$

We use the mean absolute error

$$\frac{1}{3N_\tau \cdot N^2} \sum_{i,j,n=0}^{N,N,N_\tau} |E_{z\text{numer.}}^n(i, j) - E_{z\text{true}}^n(i, j)| + |H_{x\text{numer.}}^n(i, j) - H_{x\text{true}}^n(i, j)| + |H_{y\text{numer.}}^n(i, j) - H_{y\text{true}}^n(i, j)|,$$

where the subscripts “numer.” and “true” refer to the numerical and analytical solution, respectively. The ghost nodes are easily defined using Corollary 3.5. The ghost points for H_x (see Figure 2) are defined similarly.

5.2. Comparable schemes: $C4, NC, AI^h$. We compare our proposed scheme, denoted by $C4$, with the following two schemes, which are second-order accurate in time. These schemes are obtained according to the Yee updating rules:

$$\begin{aligned} E_z^{n+1} &= E_z^n + h_\tau(D_x H_y^{n+1/2} - D_y H_x^{n+1/2}), \\ H_x^{n+3/2} &= H_x^{n+1/2} - h_\tau D_y E_z^{n+1}, \\ H_y^{n+3/2} &= H_y^{n+1/2} + h_\tau D_x E_z^{n+1}, \end{aligned}$$

where D_x and D_y are finite difference operators that approximate the first derivative on different stencils. For the derivatives in the x direction, we consider a general stencil

$$S = \frac{1}{h} \begin{pmatrix} -b & -a & a & b \\ -d & -c & c & d \\ -b & -a & a & b \end{pmatrix},$$

whereas for the derivatives in the y direction we use the transposed stencil S^t . In particular,

$$\begin{aligned} \partial_x u_{ij} &\sim \frac{c(u_{i+\frac{1}{2},j} - u_{i-\frac{1}{2},j}) + d(u_{i+\frac{3}{2},j} - u_{i-\frac{3}{2},j})}{h} + \\ &\frac{a(u_{i+\frac{1}{2},j+1} + u_{i+\frac{1}{2},j-1} - u_{i-\frac{1}{2},j+1} - u_{i-\frac{1}{2},j-1}) + b(u_{i+\frac{3}{2},j+1} + u_{i+\frac{3}{2},j-1} - u_{i-\frac{3}{2},j+1} - u_{i-\frac{3}{2},j-1})}{h}. \end{aligned}$$

For grid nodes near the boundary, we use the standard fourth-order accurate one-sided finite-difference approximation of the first derivatives.

By a Taylor expansion, we obtain second-order accuracy provided that

$$c + 3d + 2a + 6b = 1,$$

and fourth-order accuracy if the additional constraints hold:

$$c + 27d + 2a + 54b = 0, \quad (5.4a)$$

$$a + 3b = 0. \quad (5.4b)$$

We define the following stencils:

$$K_2 = \frac{1}{\Delta x} \begin{pmatrix} -b & -a & a & b \\ -d & -1 + 3d + 2a + 6b & 1 - 3d - 2a - 6b & d \\ -b & -a & a & b \end{pmatrix}, \quad (5.5)$$

$$K_4 = \frac{1}{\Delta x} \begin{pmatrix} \frac{a}{3} & -a & a & -\frac{a}{3} \\ -\frac{16a-1}{24} & -\frac{9-16a}{8} & \frac{9-16a}{8} & \frac{16a-1}{24} \\ \frac{a}{3} & -a & a & -\frac{a}{3} \end{pmatrix}. \quad (5.6)$$

The non-compact fourth-order accurate scheme that we denote NC exploits the stencil K_4 with $a=0$. Its order of accuracy is $O(h^4) + O(h_\tau^2)$.

The data-driven scheme AI^h (see Appendix A.3) uses the stencil K_2 , where the free parameters are obtained by means of a minimization process over the given training data. This scheme is of order $O(h^2) + O(h_\tau^2)$. We use this approach since it has been recently shown to reduce the numerical dispersion for the wave equation [9]. The details of the minimization process and the selected training data are detailed in Appendix A.3.

5.3. Observations. In Table 4, we verify the fourth-order accuracy of our scheme C4 and provide the rates of grid convergence for the other two (NC, AI^h) schemes as well.

In Table 5, we examine the effect of the CFL number on the mean error and verify the results of our stability analysis (Section 4). For the points-per-wavelength (PPW) ratio of 64 ($k_x = k_y = 2$), the mean error is smaller for scheme C4, as expected. Moreover, the NC scheme is more accurate than AI since it is of a higher spatial order, For the PPW ratio of approximately 6.4, the AI scheme shows a similar error to that of C4 even though it is of only second order. This is due to the fact that the AI scheme was trained on coarse grids with low number of points of points per wavelength.

In Figure 3, we examine the mean error as a function of the wave number. As expected, as the PPW ratio decreases, the C4 scheme no longer outperforms the other schemes. This is consistent with the Taylor approximation where the local truncation error depends on higher-order derivatives that increase for shorter wavelengths (larger wavenumbers $\sqrt{k_x^2 + k_y^2}$).

In Figures 4 and 5, we examine how the error behaves as a function of the time step. As expected, scheme C4 is more accurate when the wave number is low ($\sqrt{k_x^2 + k_y^2} = 2$) and the local truncation errors are relatively small. However, we see that for $k_x = k_y = 11$ the

N	NC	C4	AI^h
$k_x = k_y = 2$ (PPW 64), $r = \frac{5}{6\sqrt{2}}$			
32	1.94	5.06	2.69
64	1.98	4.98	1.89
128	1.98	4.84	1.88
256	1.99	4.48	1.93
512	2.00	4.09	1.96
$k_x = k_y = 21$ (PPW ~ 6), $r = \frac{5}{6\sqrt{2}}$			
32	0.13	0.51	0.86
64	0.81	4.80	3.32
128	1.74	4.78	1.93
256	1.96	5.09	1.35
512	1.99	4.18	1.85
$k_x = k_y = 2$, $r = \frac{1}{6\sqrt{2}}$			
32	1.31	5.21	1.88
64	1.86	4.40	1.97
128	1.97	3.96	1.99
256	2.00	3.92	1.99
512	2.00	3.94	2.00
$k_x = k_y = 21$, $r = \frac{1}{6\sqrt{2}}$			
32	0.02	0.30	0.43
64	3.17	4.28	0.55
128	7.46	4.00	1.61
256	-0.97	3.88	1.94
512	1.66	3.93	1.99

TABLE 4. Grid convergence for the three schemes we have chosen. N is the grid dimension. PPW is the points-per-wavelength ratio. $T = \frac{1}{\sqrt{2}}$, $Z = 1$.

non-compact scheme is more accurate for $r = \frac{1}{6\sqrt{2}}$ while C4 is more accurate for $r = \frac{5}{6\sqrt{2}}$ when the time step increases and as a result the temporal error is larger.

Moreover, we see that for $r = \frac{1}{6\sqrt{2}}$, the scheme NC is more accurate than AI while the situation is the opposite for $r = \frac{5}{6\sqrt{2}}$. This is not a surprise since the dispersion effects may grow as the time step increases [2].

For higher wave numbers ($\sqrt{k_x^2 + k_y^2} = 29$ and $\sqrt{k_x^2 + k_y^2} = 51$), the fourth-order accuracy of C4 and the spatial fourth-order accuracy of NC lose their advantage due to the pollution effect, and as the wave number increases the AI scheme demonstrates a similar accuracy even though it is only second-order accurate in both time and space.

r	NC	C4	AI^h
$k_x = k_y = 2$ (PPW 64)			
$\frac{1}{6\sqrt{2}}$	2.86e-05	4.06e-07	7.92e-04
$\frac{2}{6\sqrt{2}}$	1.18e-04	3.38e-07	3.86e-03
$\frac{3}{6\sqrt{2}}$	2.66e-04	2.26e-07	3.05e-03
$\frac{4}{6\sqrt{2}}$	4.73e-04	1.01e-07	1.68e-03
$\frac{5}{6\sqrt{2}}$	7.38e-04	2.49e-07	9.23e-05
$\frac{1}{\sqrt{2}}$	∞	∞	—
$k_x = k_y = 21$ (PPW ~ 6)			
$\frac{1}{6\sqrt{2}}$	1.30e-01	5.72e-02	2.57e-01
$\frac{2}{6\sqrt{2}}$	3.39e-02	4.89e-02	2.95e-01
$\frac{3}{6\sqrt{2}}$	1.39e-01	3.49e-02	2.79e-01
$\frac{4}{6\sqrt{2}}$	2.93e-01	1.58e-02	2.55e-01
$\frac{5}{6\sqrt{2}}$	2.48e-01	2.60e-02	6.48e-02
$\frac{1}{\sqrt{2}}$	∞	∞	—

TABLE 5. The error for different CFL numbers r . $T = \frac{4}{\sqrt{2}}$, $Z = 1$, $h = \frac{1}{64}$.

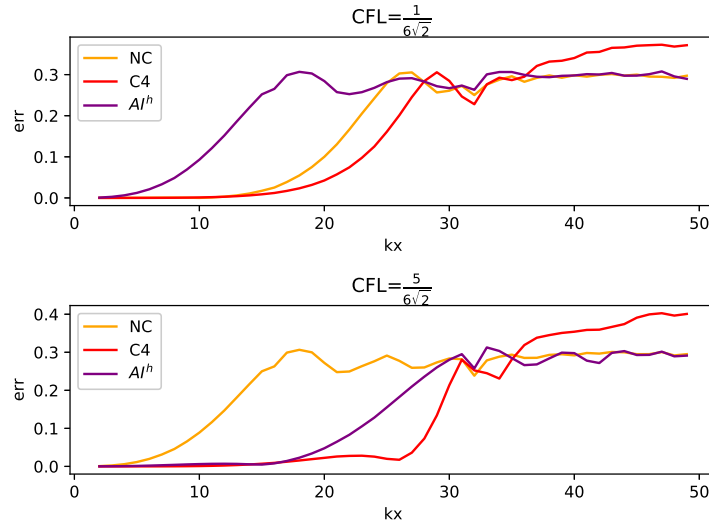


FIGURE 3. In both panels $k_y = k_x$, $T = \frac{4}{\sqrt{2}}$, $Z = 1$, and $h = \frac{1}{64}$. The points-per-wavelength ratio ranges from 64 ($\sqrt{k_x^2 + k_y^2} = 2$) to ~ 2.5 ($\sqrt{k_x^2 + k_y^2} = 50$).

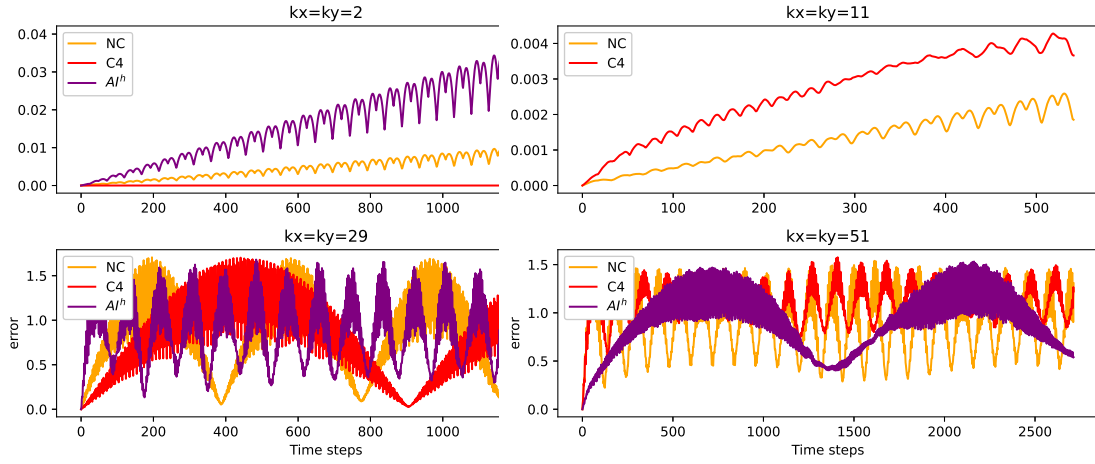


FIGURE 4. $h = \frac{1}{64}$, $r = \frac{1}{6\sqrt{2}}$, $Z = 1$.

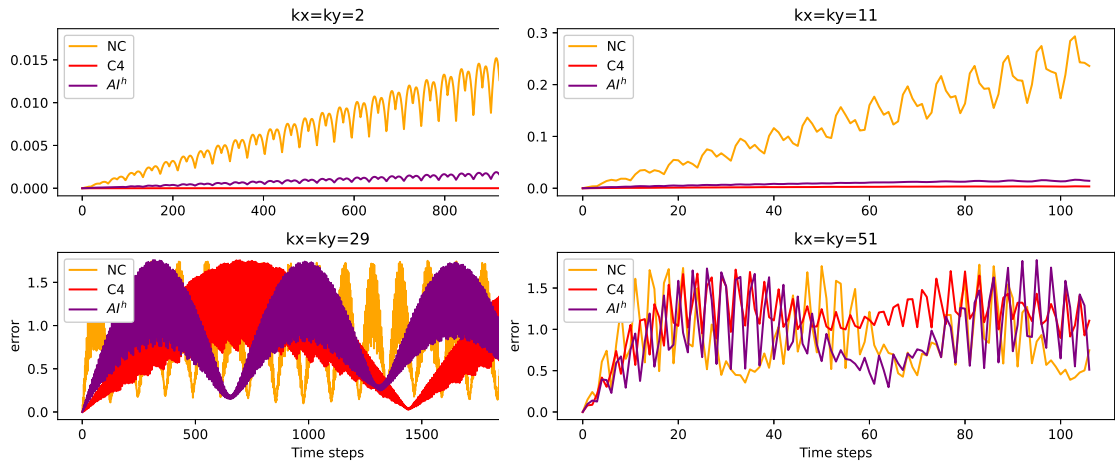


FIGURE 5. $h = \frac{1}{64}$, $r = \frac{5}{6\sqrt{2}}$, $Z = 1$.

6. CONCLUSIONS

We have constructed a compact implicit scheme for the 3D Maxwell's equations. The scheme is fourth-order accurate in both space and time and can therefore also be useful for long-time simulations, including scenarios where the PPW ratio is not very high. The scheme is compact and maintains its accuracy near the boundaries using equation-based approximations. The temporal grid is staggered, which allows us to solve 3 scalar uncoupled elliptic equations at each half-time step. That can be done in parallel with the help of the conjugate gradient method. The elliptic equations are strictly positive definite, which enables rapid convergence of the iterative scheme. With fixed CFL number, approximately three iterations of conjugate gradient are required for convergence regardless the grid size.

This is likely explained by the fact that the amount of positivity in equations (3.1) increases as the grid length decreases because the quantity $\frac{24}{h^2}$ becomes larger as h decrease and the CFL number remains fixed. Overall, the method is efficient in both CPU and memory requirements. Although we have tested numerically only 2D examples, the implementation in 3D is straightforward.

As the method we have presented is finite-difference, the pollution effect cannot be avoided completely. For higher wavenumbers, lower-order methods obtained by minimizing a certain loss function over the stencil parameters (such as data-driven) can outperform higher-order schemes.

APPENDIX A.

A.1. Operator details. Let \otimes denote the Kronecker product of matrices and let I, J, K be index sets. Let

$$D_1 = \frac{1}{h} \begin{pmatrix} -1 & 1 & 0 & 0 & 0 & \dots & 0 \\ 0 & -1 & 1 & 0 & 0 & \dots & 0 \\ 0 & 0 & -1 & 1 & 0 & \dots & 0 \\ \vdots & \ddots & \ddots & \ddots & \ddots & \ddots & \vdots \\ 0 & 0 & \dots & 0 & -1 & 1 & 0 \\ 0 & 0 & \dots & 0 & 0 & -1 & 1 \end{pmatrix} \quad (\text{A.1})$$

denote the standard central finite-difference matrix with grid size $h/2$ whose dimension equals $(m-1) \times m$, where $m \in \{|I|, |J|, |K|\}$. We define the following operators from $I \times J \times K$ to $I \times J \times K$.

$$D_x := D_1 \otimes \mathbf{1}_J \otimes \mathbf{1}_K,$$

$$D_y := \mathbf{1}_I \otimes D_1 \otimes \mathbf{1}_K,$$

$$D_z := \mathbf{1}_I \otimes \mathbf{1}_J \otimes D_1.$$

Next, we consider a fourth-order accurate approximation for first derivatives: Assume that $f(x)$ is known at N points x_0, x_1, \dots, x_{N-1} . Then, one estimates $f'(x + h/2)$ at the

$N - 1$ points $x_{\frac{1}{2}}, \dots, x_{N-3/2}$ to fourth order as:

$$\underbrace{\frac{1}{24} \begin{pmatrix} 26 & -5 & 4 & -1 & 0 & \dots & 0 \\ 1 & 22 & 1 & 0 & 0 & \dots & 0 \\ 0 & 1 & 22 & 1 & 0 & \dots & 0 \\ \vdots & \ddots & \ddots & \ddots & \ddots & \ddots & \vdots \\ 0 & 0 & \dots & 1 & 22 & 1 & 0 \\ 0 & 0 & \dots & 0 & 1 & 22 & 1 \\ 0 & 0 & \dots & -1 & 4 & -5 & 26 \end{pmatrix}}_A \begin{pmatrix} f'(x_{\frac{1}{2}}) \\ f'(x_{3/2}) \\ \dots \\ \dots \\ \dots \\ f'(x_{N-3/2}) \end{pmatrix} = \frac{1}{h} \begin{pmatrix} f(x_1) - f(x_0) \\ \dots \\ \dots \\ \dots \\ \dots \\ f(x_{N-1}) - f(x_{N-2}) \end{pmatrix} + O(h^4). \quad (\text{A.2})$$

We define the following operators from $I \times J \times K$ to $I \times J \times K$.

$$\begin{aligned} a_x^{-1} &:= A^{-1} \otimes \mathbf{1}_J \otimes \mathbf{1}_K, \\ a_y^{-1} &:= \mathbf{1}_I \otimes A^{-1} \otimes \mathbf{1}_K, \\ a_z^{-1} &:= \mathbf{1}_I \otimes \mathbf{1}_J \otimes A^{-1}, \end{aligned}$$

and

$$\begin{aligned} \delta_x &:= a_x^{-1} D_x, \\ \delta_y &:= a_y^{-1} D_y, \\ \delta_z &:= a_z^{-1} D_z. \end{aligned}$$

Finally, we define a fourth-order approximation of the curl operator as a matrix that operates on the vectorized tensor of dimension $|I| \cdot |J| \cdot |K| \times 1$:

$$\mathbf{curl}_h := \begin{pmatrix} 0 & -\delta_z & \delta_y \\ \delta_z & 0 & -\delta_x \\ -\delta_y & \delta_x & 0 \end{pmatrix}.$$

Remark A.1. By [6, section 11], $\|\mathbf{curl}_h\| \leq \frac{2\|A^{-1}\|\sqrt{3}}{h}$ and by [18], $\|A^{-1}\| \sim \frac{6}{5}$.

We recall the standard second-order finite difference matrices for the second derivative. We define the operators D_{xx}, D_{yy}, D_{zz} from $I \times J \times K$ to $I \times J \times K$ using the square matrix

$$D_2 = \frac{1}{h^2} \begin{pmatrix} -2 & 1 & 0 & 0 & 0 & \dots & 0 \\ 1 & -2 & 1 & 0 & 0 & \dots & 0 \\ 0 & 1 & -2 & 1 & 0 & \dots & 0 \\ \vdots & \ddots & \ddots & \ddots & \ddots & \ddots & \vdots \\ 0 & 0 & \dots & 1 & -2 & 1 & 0 \\ 0 & 0 & \dots & 0 & 1 & -2 & 1 \\ 0 & 0 & \dots & 0 & 0 & 1 & -2 \end{pmatrix},$$

$$\begin{aligned} D_{xx} &:= D_2 \otimes \mathbf{1}_J \otimes \mathbf{1}_K, \\ D_{yy} &:= \mathbf{1}_I \otimes D_2 \otimes \mathbf{1}_K, \\ D_{zz} &:= \mathbf{1}_I \otimes \mathbf{1}_J \otimes D_2. \end{aligned}$$

A.2. Operator estimates. Let $r = \frac{h_x}{h}$ be the CFL number. Consider the finite-difference operators

$$P_1 := - \left(\Delta_h + \frac{h^2}{6} \Upsilon_h \right) + \frac{24}{h_\tau^2} \left(1 + \frac{2}{r^2} \right),$$

and

$$P_2 := \frac{24}{h_\tau^2} \left(-1 - \frac{2}{r^2} - \frac{h^2}{12} \Delta_h \right),$$

where

$$\Delta_h \stackrel{\text{def}}{=} D_{xx} + D_{yy} + D_{zz}, \quad \Upsilon_h \stackrel{\text{def}}{=} D_{zz}D_{xx} + D_{yy}D_{zz} + D_{xx}D_{yy}.$$

Let $\sigma(\cdot)$ denote the spectrum of a given operator. The inclusion

$$\sigma(h^2 \Delta_h) \subset [-12, 0]$$

implies that

$$\frac{h_\tau^2}{24} \sigma(-P_2) \subset [1 + 2/r^2 - 1, 1 + 2/r^2].$$

The operator $\frac{h_\tau^2}{24} \left(-\Delta_h - \frac{h^2}{6} \Upsilon_h \right) + 1 + \frac{2}{r^2}$ operates on a Fourier ansatz $\exp(\sqrt{-1}(i\theta_x + j\theta_y + k\theta_z))$ by

$$1 + \frac{2}{r^2} + \underbrace{\frac{r^2}{24} \left(6 - 2(\cos \theta_x + \cos \theta_y + \cos \theta_z) - \frac{4T}{6} \right)}_S,$$

where

$$T = (\cos(\theta_z) - 1)(\cos(\theta_x) - 1) + (\cos(\theta_x) - 1)(\cos(\theta_y) - 1) + (\cos(\theta_z) - 1)(\cos(\theta_y) - 1),$$

and $-4 \leq S \leq 12$. Hence,

$$\begin{aligned} \frac{h_\tau^2}{24} \sigma(P_1) &\subset [1 + 2/r^2 - r^2/6, 1 + 2/r^2 + r^2/2], \\ \frac{h_\tau^2}{24} \sigma(-P_2) &\in [1 + \frac{2}{r^2} - 1, 1 + \frac{2}{r^2}]. \end{aligned} \tag{A.3}$$

As a result, $r < \sqrt{3 + \sqrt{21}}$ implies that $-P_2, P_1$ are positive definite and

$$0 < \frac{2}{r^2} \leq \left\| \frac{h_\tau^2}{24} P_2 \right\| \leq 1 + \frac{2}{r^2},$$

and

$$0 < 1 + \frac{2}{r^2} - \frac{r^2}{6} \leq \left\| \frac{h_\tau^2}{24} P_1 \right\| \leq 1 + \frac{2}{r^2} + \frac{r^2}{2}.$$

A.3. The data-driven scheme. We follow the approach of [9]. The general framework for a data-driven scheme can be described as follows. Let $\{(X^n, Y^n)\}_n$ be n -tuples of data-points such that for any n , $X^n \in \mathbb{R}^m$ and $Y^n \in \mathbb{R}^l$. We define a network $\mathcal{N}_{\vec{a}}$ as a function from $\mathbb{R}^m \rightarrow \mathbb{R}^l$ which depend on parameters \vec{a} . We define a loss function of the form $\mathcal{L}_{\vec{a}} := \sum_n |\mathcal{N}_{\vec{a}}(X^n) - Y^n|$ where $|\cdot|$ is a given norm between two vectors in \mathbb{R}^l . We strive to solve the problem

$$\operatorname{argmin}_{\vec{a}} \mathcal{L}_{\vec{a}}$$

and then obtain the optimal parameters \vec{a} and the corresponding optimal network $\mathcal{N}_{\vec{a}}$. The minimization process can be done using several variations of the gradient descent method.

In our framework, we wish to find the optimal parameters a, b, d for evaluation of the first derivative using the stencil

$$K_2 = \frac{1}{\Delta x} \begin{pmatrix} -b & -a & a & b \\ -d & -1 + 3d + 2a + 6b & 1 - 3d - 2a - 6b & d \\ -b & -a & a & b \end{pmatrix}$$

in Yee updating rules (see subsection 5.2). The network will be a function that takes a solution $\mathbf{E}^n, \mathbf{H}^{n+1/2}$ and returns $\mathbf{E}^{n+1}, \mathbf{H}^{n+3/2}$ using Yee updating rules. We generate a data set of analytical solutions using (5.3a) as follows. We fix $h = \frac{1}{16}$, CFL number r and the corresponding h_τ . We also fix the final time T . The number of spatial grid points is then denoted by N and the number of times steps is denoted by N_τ . For any (k_x, k_y) in $\{12, 13, 14, 15\}^2$ we generate analytical solutions E_z, H_x, H_y defined by (5.3a). For any $0 \leq n \leq N_\tau$ we let $E_{z_{k_x, k_y, \text{true}}}^n, H_{x_{k_x, k_y, \text{true}}}^n, H_{y_{k_x, k_y, \text{true}}}^n$ be the corresponding values of the analytical solutions evaluated at the time $t = nh_\tau$. We let

$$X^{n, k_x, k_y} := (E_{z_{k_x, k_y, \text{true}}}^n, H_{x_{k_x, k_y, \text{true}}}^n, H_{y_{k_x, k_y, \text{true}}}^n).$$

Next, we build the network, $\mathcal{N}_{a,b,d}$, which takes a numerical solution at time step n , and outputs the solution at time $n+1$ evaluated using Yee updating rules with the stencil K_2 .

A single data point in our data set is then defined by $(\text{input}^{n, k_x, k_y}, \text{output}^{n, k_x, k_y})$ where

$$\text{input}^{n, k_x, k_y} = X^{n, k_x, k_y}$$

and

$$\text{output}^{n, k_x, k_y} = (X^{n+1, k_x, k_y}, X^{n+2, k_x, k_y}, X^{n+3, k_x, k_y}).$$

We omit the superscripts k_x, k_y from now on.

The loss function is then defined over all data points as follows:

$$\mathcal{L}_{a,b,d} = \sum_n |X^{n+1} - \mathcal{N}(X^n)| + |X^{n+2} - \mathcal{N}(\mathcal{N}(X^n))| + |X^{n+3} - \mathcal{N}(\mathcal{N}(\mathcal{N}(X^n)))| \quad (\text{A.4})$$

where $|\cdot|$ in (A.4) is taken to be the mean absolute error between two vectors. The loss function is minimized using Adam optimizer and Keras [4] over the data points with the usual splitting routine of train, test, and validation sets.

REFERENCES

- [1] Bayliss, A., Goldstein, C.I. and Turkel, E., 1985. On accuracy conditions for the numerical computation of waves. *Journal of Computational Physics*, 59(3), pp. 396-404.
- [2] Blinne, A., Schinkel, D., Kuschel, S., Elkina, N., Rykovanov, S.G. and Zepf, M., 2018. A systematic approach to numerical dispersion in Maxwell solvers. *Computer Physics Communications*, 224, pp. 273-281.
- [3] Britt, S., Tsynkov, S. and Turkel, E., 2011. Numerical simulation of time-harmonic waves in inhomogeneous media using compact high order schemes. *Communications in Computational Physics*, 9(3), pp. 520-541.
- [4] Chollet, F. & others, 2015. Keras. Available at: <https://github.com/fchollet/keras>.
- [5] Deraemaeker, A., Babuška, I. and Bouillard, P., 1999. Dispersion and pollution of the FEM solution for the Helmholtz equation in one, two and three dimensions. *International journal for numerical methods in engineering*, 46(4), pp. 471-499.
- [6] Gustafsson, B., Kreiss, H.O. and Olinger, J., 1995. *Time dependent problems and difference methods* (Vol. 24). John Wiley & Sons.
- [7] Gottlieb, D. and Yang, B., 1996, March. Comparisons of staggered and non-staggered schemes for Maxwell's equations. In *12th Annual Review of Progress in Applied Computational Electromagnetics* (Vol. 2, pp. 1122-1131).
- [8] Kreiss, H.O. and Olinger, J., 1972. Comparison of accurate methods for the integration of hyperbolic equations. *Tellus*, 24(3), pp. 199-215.
- [9] Ovidia, O., Kahana, A. and Turkel, E., 2022. A Convolutional Dispersion Relation Preserving Scheme for the Acoustic Wave Equation. arXiv preprint arXiv:2205.10825.
- [10] L. D. Landau and E. M. Lifshitz, 1975. *Course of Theoretical Physics, Vol. 2, The Classical Theory of Fields*, Fourth ed., Pergamon Press, Oxford.
- [11] L. D. Landau and E. M. Lifshitz, 1984. *Course of Theoretical Physics. Vol. 8, Electrodynamics of Continuous Media*, Pergamon International Library of Science, Technology, Engineering and Social Studies, Pergamon Press, Oxford.
- [12] Leis, R., 2013. *Initial boundary value problems in mathematical physics*. Courier Corporation.
- [13] Sakkaplangkul, P. and Bokil, V., 2021. Convergence analysis of Yee-FDTD schemes for 3D Maxwell's equations in linear dispersive media. *International journal of numerical analysis and modeling*, 18(4).
- [14] Singer, I. and Turkel, E., 1998. High-order finite difference methods for the Helmholtz equation. *Computer methods in applied mechanics and engineering*, 163(1-4), pp. 343-358.
- [15] Stern, A., Tong, Y., Desbrun, M. and Marsden, J.E., 2015. Geometric computational electrodynamics with variational integrators and discrete differential forms. *Geometry, Mechanics, and Dynamics: The Legacy of Jerry Marsden*, pp. 437-475.
- [16] Taflov, A., Hagness, S.C. and Picket-May, M., 2005. *Computational electromagnetics: the finite-difference time-domain method*, Artech house, Boston 1998.
- [17] Yee, K., 1966. Numerical solution of initial boundary value problems involving Maxwell's equations in isotropic media. *IEEE Transactions on antennas and propagation*, 14(3), pp. 302-307.

- [18] Yefet, A. and Turkel, E., 2000. Fourth order compact implicit method for the Maxwell equations with discontinuous coefficients. *Applied Numerical Mathematics*, 33(1-4), pp. 125-134.
- [19] Yefet, A. and Petropoulos, P.G., 2001. A staggered fourth-order accurate explicit finite difference scheme for the time-domain Maxwell's equations. *Journal of Computational Physics*, 168(2), pp. 286-315.

SCHOOL OF MATHEMATICAL SCIENCES, TEL-AVIV UNIVERSITY, TEL-AVIV 6997801, ISRAEL
Email address: `idanversano@tauex.tau.ac.il`

SCHOOL OF MATHEMATICAL SCIENCES, TEL-AVIV UNIVERSITY, TEL-AVIV 6997801, ISRAEL
Email address: `turkel@tauex.tau.ac.il`

NORTH CAROLINA STATE UNIVERSITY, BOX 8205, RALEIGH, NC 27695, USA.
Email address: `tsynkov@math.ncsu.edu`